

See discussions, stats, and author profiles for this publication at: <http://www.researchgate.net/publication/276149220>

Evidence for photochemical production of reactive oxygen species in desert soils

ARTICLE *in* NATURE COMMUNICATIONS · MAY 2015

Impact Factor: 11.47 · DOI: 10.1038/ncomms8100 · Source: PubMed

READS

36

11 AUTHORS, INCLUDING:



Henry J Sun

Desert Research Institute

34 PUBLICATIONS 903 CITATIONS

SEE PROFILE



Konstantinos Grintzalis

22 PUBLICATIONS 241 CITATIONS

SEE PROFILE



Eleni Koutsopoulou

University of Patras

10 PUBLICATIONS 21 CITATIONS

SEE PROFILE



G.E. Christidis

Technical University of Crete

48 PUBLICATIONS 690 CITATIONS

SEE PROFILE

ARTICLE

Received 14 Jul 2014 | Accepted 1 Apr 2015 | Published 11 May 2015

DOI: 10.1038/ncomms8100

Evidence for photochemical production of reactive oxygen species in desert soils

Christos D. Georgiou¹, Henry J. Sun², Christopher P. McKay³, Konstantinos Grintzalis¹, Ioannis Papapostolou¹, Dimitrios Zisimopoulos¹, Konstantinos Panagiotidis¹, Gaosen Zhang⁴, Eleni Koutsopoulou⁵, George E. Christidis⁶ & Irene Margiolaki¹

The combination of intense solar radiation and soil desiccation creates a short circuit in the biogeochemical carbon cycle, where soils release significant amounts of CO₂ and reactive nitrogen oxides by abiotic oxidation. Here we show that desert soils accumulate metal superoxides and peroxides at higher levels than non-desert soils. We also show the photo-generation of equimolar superoxide and hydroxyl radical in desiccated and aqueous soils, respectively, by a photo-induced electron transfer mechanism supported by their mineralogical composition. Reactivity of desert soils is further supported by the generation of hydroxyl radical via aqueous extracts in the dark. Our findings extend to desert soils the photogeneration of reactive oxygen species by certain mineral oxides and also explain previous studies on desert soil organic oxidant chemistry and microbiology. Similar processes driven by ultraviolet radiation may be operating in the surface soils on Mars.

¹Department of Biology, University of Patras, Patras 26504, Greece. ²Desert Research Institute, Las Vegas, Nevada 89119, USA. ³NASA Ames Research Center, Moffett Field, California 94035, USA. ⁴Cold and Arid Regions Environmental and Engineering Research Institute, Chinese Academy of Sciences, Lanzhou 73000, China. ⁵Laboratory of Electron Microscopy and Microanalysis, University of Patras, Patras 26500, Greece. ⁶Department of Mineral Resources Engineering, Technical University of Crete, Chania 73100, Greece. Correspondence and requests for materials should be addressed to C.D.G. (email: c.georgiou@upatras.gr).

In most ecosystems, microorganisms carry out mineralization of soil organic matter. In desert soils, however, non-biological and biological organic decomposition can be comparable in magnitude. For example, soils from the Atacama Desert, Chile, can oxidize D-alanine and L-glucose at significant rates, although terrestrial organisms do not utilize these enantiomers^{1,2}. In the Mojave Desert, California, nitrogen oxide (NO_y) gases are emitted from desiccated soils³ at rates comparable to wet soils only if the soils are irradiated by sunlight. In other arid and semi-arid locations, photochemical degradation reportedly accounts for 60% of plant litter decomposition⁴. Studies on the photochemical oxidation of xenobiotic organic carbon (herbicides, insecticides and pesticides) in agricultural soils suggested that ¹O₂ generated by sunlight via the photosensitization of soil organics (and possibly of Ti- and Zn-oxides) to be the main oxidant⁵. The involvement of other reactive oxygen species (ROSS) such as superoxide (O₂⁻) and hydroxy (·OH) radical has been hypothesized as well^{6–11}. OH is postulated to result indirectly from the reaction of water with humic substances in the excited triplet state or from degradation of H₂O₂ by transition metal (Me_{tr}) cations such as Fe³⁺ via a photo-Fenton reaction¹⁰. However, the photochemical oxidative process and its components are not well understood because of a lack of methods for the detection of the involved ROS in soils and their very short life (1 ns to 1 μs (ref. 12)).

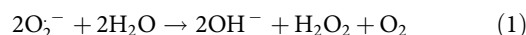
Photogenerated ROS have been identified in laboratory studies on mineral oxides (mainly TiO₂) exposed to ultraviolet radiation: atomic oxygen radical anion (O⁻), ozone radical anion (O₃⁻, and possibly O₄⁻), O₂⁻ and ·OH^{13–15}. The postulated process in these studies involves ultraviolet-induction of electron mobilization from the oxide surface and its subsequent capture by O₂ to form oxygen radical surface adsorbates¹⁶. This photo-induced mechanism is also supported by the previously shown generation of O₂⁻ in ultraviolet-exposed plagioclase feldspars¹⁷. Singlet oxygen (¹O₂) also has been identified^{18,19} and may oxidize soil organics via intermediate oxidant products but is not adsorbed on mineral surfaces because it is uncharged. Degradation of organic compounds, mainly via ·OH, can be catalysed by the photochemistry (via reduction) of iron (III) species such as Fe(OH)₃, FeOOH and Fe₂O₃ (ref. 20), besides TiO₂-mineral oxides.

Here we show that metal superoxides and peroxides accumulate in topsoils of the Atacama and Mojave deserts (at mid-summer sunlight irradiance 800–1,000 W m⁻²) at a 10-fold higher level than in a non-arid control site. Moreover, we show that desiccated and aqueous desert soils photogenerate equimolar O₂⁻ adsorbates and ·OH, respectively, and also that the reactivity of desert soils is associated with the generation of ·OH and the concomitant decrease of soil H₂O₂ in their aqueous extracts in the dark, possibly via the Fenton reaction due to the presence of Me_{tr} in these soils. For this study, new methods enable the identification of soil O₂⁻, H₂O₂ and ·OH. These methods are not yet suitable, however, for *in situ* studies on the

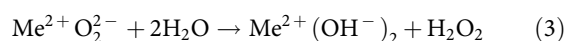
seasonal and soil depth-dependent formation rates of detected soil oxidants. Moreover, their specificity restricts the evaluation of only a fraction of the photogenerated ROS involved in the oxidative desert soil chemistry. Although the elucidation of the entire model of desert soil ROS photogeneration is not possible with the available methods, they unveil some key steps as they take place by a photo-induced electron transfer mechanism. In addition, our selected soil desert sites are among the most studied of all the world's arid locations^{1,21,22}, and thus provide a good basis for considering the environmental effects of aridity on the photochemical production of ROS in desert soils.

Results

Detection and stability soil O₂⁻/peroxides and detection of Me_{tr}. We extracted soil metal superoxides as O₂⁻ from desiccated Atacama and Mojave Desert topsoils by acetonitrile and quantified fluorometrically by a modified hydroethidine (HE)-based assay^{23,24}, and the identity of O₂⁻ and validity of the HE-based assay were verified by a second assay^{25,26}, a modification of the superoxide dismutase (SOD)-inhibited equimolar reduction of cyt. c by O₂⁻ (Methods, Supplementary Methods). The methodological baseline for O₂⁻ detection was determined in H₂O-prewashed and dried soil, a treatment that destroys O₂⁻ by dismutation¹²:



Soil metal peroxides (peroxides/hydroperoxides) were quantified upon aqueous extraction as H₂O₂ (their hydrolysis product shown in reactions 2–4; refs 27,28):



Soil metal peroxides can be present, however, in mixture with metal superoxides that on aqueous extraction also release H₂O₂ (reaction 1). Thus, the extracted soil H₂O₂ is the sum of two fractions that can be quantitatively differentiated. The first H₂O₂ fraction results from equimolar hydrolysis of metal peroxides (equations 2–4). The second is differentiated from the first because it results from dismutation of ×2 molar metal superoxides (equation 1). Total soil H₂O₂ extracted from metal superoxides plus peroxides was quantified by a modification of the Fe²⁺-xylenol orange assay (Methods, Supplementary Methods), using catalase as control²⁹.

Atacama and Mojave Desert soils contained ~2.0 nmol O₂⁻ g⁻¹ (that is, metal superoxides). In contrast, soils from a non-arid control location contained an order of magnitude less concentration of ~0.2 nmol g⁻¹ (Table 1). However, the dry desert soil is conducive to preservation of O₂⁻, while constantly humid soils are not (because of reaction 1). Even in the deserts, given the extreme labile nature of O₂⁻, only a small fraction would be

Table 1 | Soil metal superoxides, total superoxides/peroxides (H₂O₂) and Fe³⁺.

Soil oxidants*	Atacama Desert sites*		Mojave Desert sites*		Control site*
	1	Yungay	Basalt	+ CIMA sand	
O ₂ ^{-†}	1.8 ± 0.6 (0.03)	1.9 ± 0.3 (0.03)	2.3 ± 0.4 (0.04)	2.0 ± 0.3 (0.03)	0.15 ± 0.06 (0.002)
H ₂ O ₂	14 ± 2 (0.05)	19 ± 2 (0.6)	110 ± 9 (4)	5 ± 0.7 (0.4)	0.2 ± 0.01 (0.01)
Fe ^{3+†}	20 ± 2 (1.2)	10 ± 1 (0.6)	10 ± 3 (0.6)	12 ± 2 (0.6)	0.2 ± 0.03 (0.01)

*Metal superoxides are expressed as soil O₂⁻ (nmol g⁻¹) and total superoxides/peroxides as their hydrolysis product H₂O₂ (in nmol g⁻¹ soil). Soil Fe³⁺ concentration is expressed in nmol g⁻¹. Data are mean values ± standard error from at least five replicates. Numbers in parentheses are in ppm.

†Values for soil O₂⁻ are averages of the mean values obtained by the HE-based and the SOD-inhibited reduction of cytochrome c-based soil O₂⁻ assays. For statistical comparison of both assays, the within-day % coefficient variation is <3.7% and the variance of intermediate precision (or between day repeatability) is <4.8%.

stabilized in soils. The Mojave and Atacama Desert soils also contain metal peroxides (Table 1) because the concentration levels of the extracted total soil H_2O_2 are 5–95 times higher than the H_2O_2 expected from the (dis)mutation of the detected soil metal superoxides. The levels of H_2O_2 we detected in both Atacama Desert sites are similar to those previously reported¹.

The detected soil metal superoxides and peroxides were stable even when the desiccated desert soils were heated at 200 °C for 1 h. This agreed with the finding that the desert soils retained ~50% of their initial concentrations in metal superoxides and peroxides after storage for 1 year (desiccated in the dark at ~16 °C; data not shown). The extracted H_2O_2 was not stable through time, however, as almost 50% was destroyed within 1 day in the dark (Fig. 1a). This could be because of its decomposition to $\cdot\text{OH}$ by co-extracted Me_{tr} via the Fenton reaction^{12,30}, as supported by the identification of Fe and other Me_{tr} (for example, Cu, Cr, Co, Ni) in these soils (Tables 1 and 2) and the participation of these in the Fenton reaction³¹. Indeed, desert soil H_2O_2 extracts generated $\cdot\text{OH}$ through time (Fig. 1b, Methods, Supplementary Methods), the rate of which in the presence of soil decreased by ~6-fold probably because of $\cdot\text{OH}$ scavenging by soil organics³² and/or metal (Me) ions (via the general reaction: $\cdot\text{OH} + \text{Me}^{n+} + \text{H}_2\text{O} \rightarrow \text{Me}^{n+} + \text{OH}^- \rightarrow \text{Me}^{(n+1)+} + \text{OH}^-$; ref. 33).

Photogeneration of soil O_2^- and $\cdot\text{OH}$, and mineral analysis.

ROS were photogenerated (by natural sunlight and ultraviolet C) by desiccated soils. Before exposure soils also were washed to

remove any potentially interfering soil inorganics (for example, perchlorates and nitrates known to exist in these deserts^{34,35}) and organics (for example, photosensitizers, ROS scavengers; Methods). Soil O_2^- and H_2O_2 (peroxides) concentrations almost doubled or tripled (above baseline; 1.5 and 0.7 nmoles g^{-1} , respectively) during the first hour of soil irradiation (Fig. 2). A similar trend for O_2^- generated on ultraviolet-irradiated plagioclase feldspar minerals has been observed previously¹⁷. Longer irradiation (up to 6 h) resulted in a concentration plateau for O_2^- (similarly for H_2O_2), irrespective of the radiation source (although somewhat higher for the more effective ultraviolet C), which could be due to the saturation of the positively charged sites on the soil surface by the O_2^- anion. The concentration of the soil photogenerated O_2^- (Fig. 2a) was approximately twice that of H_2O_2 (Fig. 2b). This $\text{O}_2^-/\text{H}_2\text{O}_2$ ratio fits the stoichiometry of the dismutation of O_2^- (reaction 1), which indicates that O_2^- is the main soil oxidant formed during sunlight/ultraviolet C exposure.

We analysed the mineral substrates potentially involved in the photogeneration of ROS by the Atacama and Mojave Desert and control soils both in the bulk and the clay fractions of the samples (Methods, Supplementary Methods). All the samples contained plagioclase feldspar with composition that varied from albite to labradorite. Clay minerals were most abundant in the control soil, absent from the Mojave Desert basalt, and found in traces in the remaining samples, in accordance with the Loss On Ignition data in Table 2. All the soils contain traces of Fe-Ti- and/or Fe-Mn- and/or Fe-oxides and/or Ti-oxides.

It has been established that aqueous TiO_2 photogenerate O_2^- and $\cdot\text{OH}$ ^{15,36}, the latter being photogenerated by aqueous TiO_2

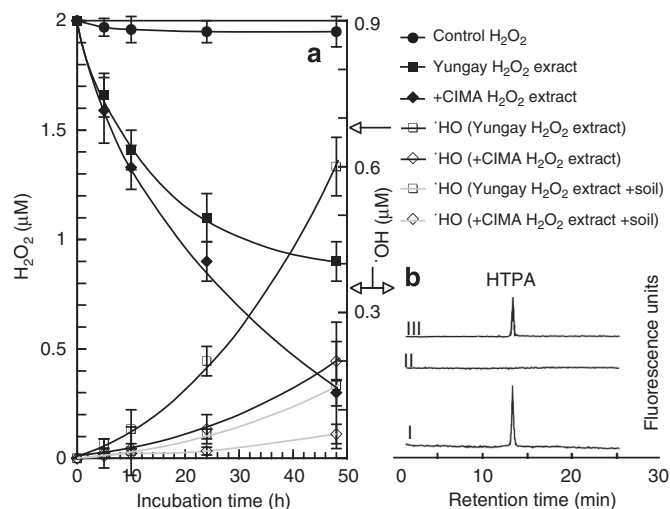


Figure 1 | Instability of acid-extracted soil H_2O_2 and generation of $\cdot\text{OH}$.

Soil H_2O_2 results from the dismutation/hydrolysis of metal superoxides/peroxides, respectively. (a) Decreasing exponential solid line curves depict the change of 10 mM H_3PO_4 -extracted soil H_2O_2 concentration (initially adjusted to 2 μM , and in the absence of the extracted soil) from the Mojave and Atacama +CIMA and Yungay sites (filled rhombs and squares), respectively, versus time, against a 2.0 μM H_2O_2 (in 10 mM H_3PO_4) control solution (filled circles). Increasing exponential line curves depict the generation (versus time) of $\cdot\text{OH}$ in the H_2O_2 extracts from the same Mojave and Atacama sites (open rhombs and squares, respectively) in the absence and presence of soils (solid and dotted lines, respectively).

(b) $\cdot\text{OH}$ was detected from its reaction with TPA (added to the H_2O_2 extracts at 2 mM) and the equimolar production of the specific fluorescent product HTPA⁷⁰. HTPA was quantified and identified fluorometrically by HPLC (I, using as controls the $\cdot\text{OH}$ scavenger DMSO, II, and pure HTPA, III). Similar data (not shown) were obtained for H_2O_2 extracted from total peroxides from the other tested Atacama and Mojave Desert soil sites. Error bars designate s.d.

Table 2 | Bulk sample chemical analysis.

Major elements (wt %)	Atacama desert		Mojave desert		Control site
	Site 1	Yungay	Basalt	+ CIMA	
SiO_2	63.10	61.80	46.31	67.07	55.39
TiO_2	1.11	0.81	2.48	0.66	0.53
Al_2O_3	15.98	13.45	15.80	14.05	9.21
$\text{Fe}_2\text{O}_3\text{t}$	5.26	5.43	10.29	4.47	4.02
MnO	0.07	0.07	0.13	0.05	0.08
MgO	1.20	1.52	7.31	1.43	2.03
CaO	4.55	5.31	9.28	3.22	12.13
Na_2O	3.99	3.82	4.09	3.50	1.32
K_2O	2.41	2.37	1.96	3.10	1.62
P_2O_5	0.16	0.16	0.68	0.17	0.10
LOI*	2.09	5.73	1.39	2.30	12.92
Total	99.92	100.47	99.72	100.02	99.35
Trace elements (p.p.m.)					
V	172	164	215	76	78
Cr	38	31	146	27	202
Co	8	11	164	7	17
Ni	14	15	120	14	100
Cu	50	81	89	21	46
Zn	50	79	89	47	105
Rb	62	88	41	107	73
Sr	390	604	807	448	195
Y	17	20	35	27	22
Zr	201	185	320	340	150
Ba	681	744	599	711	230
La	23	30	41	36	21
Ce	33	44	73	71	42
Nd	18	17	29	39	24
Pb	18	39	16	33	48
Th	7	9	5	12	8

*LOI, loss on ignition.

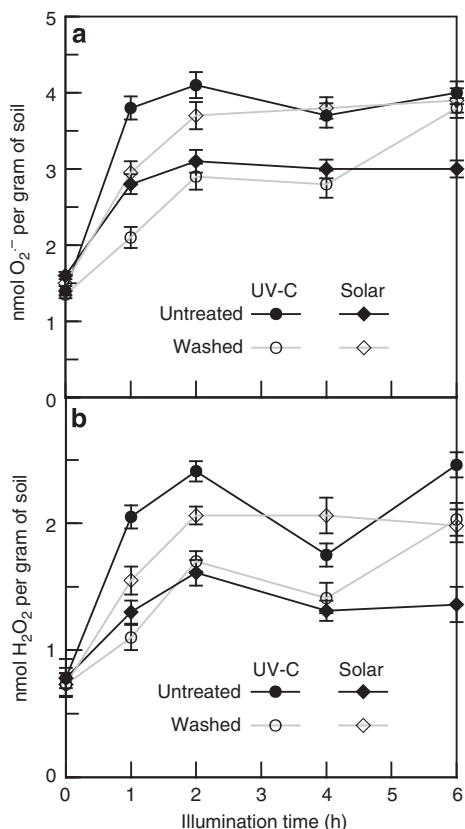


Figure 2 | Photochemical formation of ROS in desert soils. (a) O_2^- was generated in the Mojave Desert +CIMA site (untreated or washed and then dried), which was exposed to solar (natural sunlight) and ultraviolet C irradiation versus exposure time. (b) Generation of total metal superoxides/peroxides (expressed as H_2O_2) in the same +CIMA site under irradiation conditions as in a. Similar data (not shown) were obtained in the other tested desert/control sites. Error bars designate s.d.

films as well^{37,38}. The presence in the tested desert soils of Ti-based transition metal oxides prompted us to investigate whether these soils photogenerate $\cdot\text{OH}$ under aqueous conditions. Here we show that both Atacama and Mojave soils (0.2 g, prewashed from any soluble inorganic and organic constituents) photogenerate an average of $3.2 \text{ nmol } \cdot\text{OH h}^{-1}$ (Fig. 3) upon exposure to 180 W m^{-2} 400–700 nm (or 18% that of sunlight). This rate is proportional to light intensity as well (data not shown), obeying zero-order reaction rate kinetics as in aqueous TiO_2 film photocatalysis³⁸. We identified $\cdot\text{OH}$ and quantified its rate of photogeneration by a modification of the terephthalic acid (TPA)-based assay^{37,38} and by the ~ 15 -fold rate decrease caused by the $\cdot\text{OH}$ scavenger dimethyl sulfoxide (DMSO; Methods). $\cdot\text{OH}$ is not photogenerated by exposing a control H_2O_2 solution, given that H_2O_2 is released from metal superoxides/peroxides under aqueous conditions.

Generation of $3.2 \text{ nM } \cdot\text{OH}$ in 1 h by 0.2 g soil exposed to 180 W m^{-2} or 18% that of sunlight corresponds to $\sim 1 \text{ nmol g}^{-1}$ for 1 h exposure to sunlight (see Supplementary Methods). This is similar to the plateau rate of $1.45 \text{ nmol O}_2^- \text{ g}^{-1}$ that is generated by desiccated (and prewashed) desert soils after exposure to sunlight for 1 h (Fig. 2a). This near 1:1 molar $\text{O}_2^-/\cdot\text{OH}$ ratio is in agreement with the mechanism of TiO_2 photocatalysis^{15,36}, which assumes equimolar $\cdot\text{OH}$ and O_2^- aqueously generated; the latter also being photogenerated in desiccated soils by the same mechanism (Fig. 4). The ratio 1:1.5 deviation from the equimolar ratio could be due to various factors

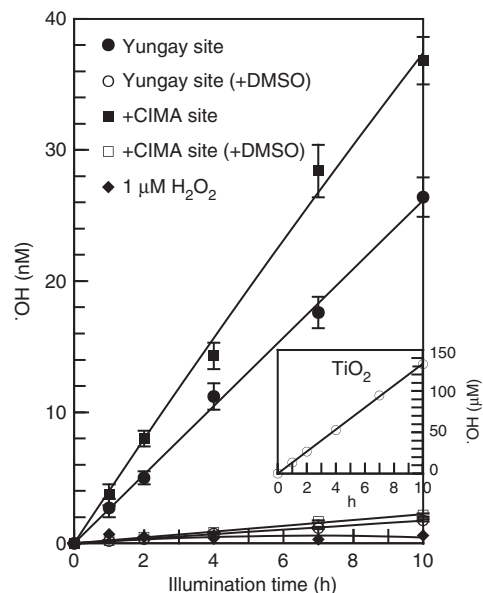


Figure 3 | Photogeneration of $\cdot\text{OH}$ by desert soils under aqueous conditions. Soils (from the Atacama Yungay site and the Mojave +CIMA site) were extensively washed and exposed to light (400–700 nm), against $\pm 100 \text{ mM}$ DMSO ($\cdot\text{OH}$ scavenger) and an H_2O_2 control, using commercial TiO_2 (inset) as additional control, given its presence in the tested desert soils. The other tested desert/control sites gave similar data (not shown). Error bars designate s.d.

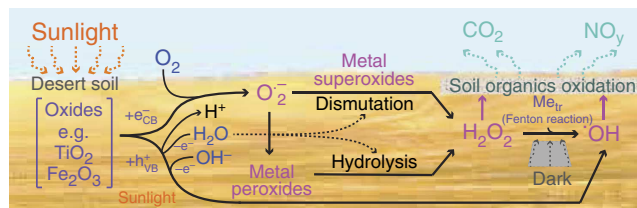


Figure 4 | Photochemical mechanism of desert soil oxidizing action.

Sunlight radiation of soils generates unpaired electrons that convert O_2 to O_2^- . This radical can be initially adsorbed on the surface of soils and stabilized in the long term as metal superoxides and peroxides. These can be converted under aqueous conditions (via dismutation and hydrolysis, respectively) to H_2O_2 , which can be converted subsequently to hydroxyl radical ($\cdot\text{OH}$) in the dark by reaction with reduced soil transition metals (Me_{tr}). A second route of $\cdot\text{OH}$ generation may involve a single electron abstraction from H_2O or OH^- by an h^+_{VB} hole (see text). $\cdot\text{OH}$ (and also H_2O_2 and O_2^- , although to a lesser degree as weak oxidants) can then oxidize soil organics possibly to CO_2 and NO_y .

such as the non-aqueous/aqueous generation of additional ROS species (for example, O^- , O_3^- , O_4^- ; refs 13–15), the not accounted ultraviolet component of natural sunlight, and the possible incomplete trapping of $\cdot\text{OH}$ by the assay reagent TPA. Generation of $\cdot\text{OH}$ by photodissociated H_2O_2 , under the employed experimental conditions, may be negligible as shown by the corresponding assay control (Fig. 3). The aqueous photogeneration of $\cdot\text{OH}$ by metal oxides in desert soils also was supported by our control experiment with TiO_2 . Tested at a quantity equivalent to its w% concentration in the soils (Table 2), TiO_2 produced $\cdot\text{OH}$ at $\sim 13 \mu\text{M h}^{-1}$ (Fig. 3 inset). This $\sim 4,000$ -fold higher rate compared with the desert soils is because of the very small particle size of TiO_2 (photocatalysis grade, $< 30 \text{ nm}$ in size; ref. 39), that results in a highly disordered structure and high

specific surface area compared with the natural TiO₂ polymorphs and ilmenite (that is, Fe–Ti oxides) found in the tested soils.

Discussion

Superoxide radical is photogenerated in desert soils (Fig. 2a) and stabilized initially as surface-saturating desiccated anionic adsorbate, given that it is the least reactive hence the most stable species formed by ultraviolet exposure¹⁷. Long-term diffusion of O₂^{•−} may be the subsequent stabilization process, as metal superoxides and peroxides were detected in the Atacama and Mojave Desert soils. This is in agreement with the finding that the average concentration of metal superoxides in a basalt rock (pulverized) from the Mojave Desert + CIMA field is similar to their concentration in the surrounding sand (Table 1), suggesting a long-term O₂^{•−} diffusion inside basalt rocks. Such diffusion through soils does not occur within the short irradiation period used in our and similar studies (with labradorite), since this is considered geologically very short¹⁷.

In general, the main conditions under which stable O₂^{•−} is formed on the surface of metal oxides and zeolites are (i) photoinduced electron transfer, (ii) direct surface-oxygen electron transfer, (iii) surface intermolecular electron transfer and (iv) the decomposition of H₂O₂ (ref. 40). The photo-induced electron transfer mechanism (Fig. 4) could involve ejection from transition or non-transition metal oxides (for example, TiO₂, Fe₂O₃ (ref. 20), or ZnO (ref. 41), respectively) of an electron (e[−]_{CB}) into its CB (conduction band) from its valence band (VB), and its transfer to O₂ with concomitant generation of O₂^{•−}, leaving a positively charged hole (h⁺_{VB}) at the band edge of the VB. In addition to O₂^{•−}, an adsorbed [•]OH may be formed on the oxide surface, from an e[−] abstracted by the h⁺_{VB} hole from H₂O or OH[−] (refs 15,36,40,42). Nonetheless, O₂ may not be the only acceptor of the photogenerated single electrons, as ¹O₂ also possesses sufficient one-electron reduction potential to form O₂^{•−} (ref. 43). Then, the photogenerated O₂^{•−} could be adsorbed on the surface of minerals where it could saturate their positively charged sites. In the long term, O₂^{•−} may migrate via diffusive transport to greater depths in the soils, where it may stabilize as metal superoxides and peroxides (Table 1).

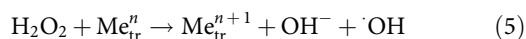
Metal superoxides/peroxides are better preserved (protected from dismutation/hydrolysis, respectively) in desiccated soils than in soils containing water⁴². This, in turn, depends on the clay mineral composition. Swelling clay minerals (smectite and vermiculite), that were more abundant in the control site soil, readily adsorb H₂O molecules, thus contributing to greater water adsorption⁴⁴ and possibly to lower stability of O₂^{•−} and metal peroxides. This assumption could explain the observed 10-fold lower concentration of metal superoxides and the much lower concentration of metal peroxides in the control soil compared with the desert soils (Table 1).

Moreover, the presence of albite and labradorite plagioclase in the Atacama and Mojave Desert soils, respectively, is in agreement with the previously proposed ultraviolet-induced mechanism of O₂^{•−} generation by these minerals^{17,42}. The same mechanism might also apply for the albite-bearing control site soil. Also, metal superoxides and peroxides may be continuously photogenerated in all soils because TiO₂, Fe-oxides and Fe-Ti-oxides—present in the tested soils and typical of desert soils⁴⁵—are known to be involved in the photogeneration process of O₂^{•−} (refs 13–15,17,36). In addition to Ti (in Ti- and/or Fe-Ti-oxides) as well as Fe and Mn (in Fe- and/or Mn-oxides either free or impurities in silicate minerals), the long-term stabilization process for adsorbed soil O₂^{•−} as metal superoxides and peroxides also may involve (besides Ti⁴⁶) the exchangeable metals Ca, Na and K that are present in smectite. Specifically, O₂^{•−} may be stabilized as (i) metal

superoxides such as KO₂ and NaO₂, (ii) metal peroxides such as Na₂O₂, CaO₂, K₂O₂ and TiO₃•2H₂O and TiO₂•2H₂O (both less water soluble) that are usually formed by the reaction of the metal with H₂O₂ and (iii) metal hydroperoxides such as NaOOH, (KOOH)₂•3H₂O and Ti(OH)₃OOH^{27,28}.

The photochemical production of O₂^{•−} as soil adsorbate and stabilized as metal superoxides/peroxides could explain the reactivity of desert soils with organics (Fig. 4) under several considerations. Soil H₂O₂ (for example, aqueously generated via reactions 1–4) can decompose carbohydrates to formic acid and ultimately to CO₂ (ref. 47). The release of NO_y from the Mojave Desert soil³ and N₂O from the Atacama Desert soil⁴⁸) could have resulted from [•]OH by the following mechanism: [•]OH can oxidize amino acids with ammonia as a byproduct. Ammonia can be further oxidized by [•]OH to amidogen radical⁴⁹, that can subsequently react with O₂ to form nitric oxide radical ([•]NO), dioxide radical ([•]NO₂) and N₂O (refs 49–51).

Hydroxyl radical can be generated from H₂O₂ (the product of dismutation/hydrolysis of metal superoxides/peroxides, respectively) either by the Fenton reaction (5) catalysed by Me_{tr} or by O₂^{•−} via the Me_{tr}-catalysed Haber–Weiss reaction (6)³⁰:



The Fenton mechanism is considered probable because Me_{tr} (Fe³⁺ and trace elements Cu, Cr, Co and Ni) were identified in Mojave and Atacama Desert soils (Tables 1 and 2). Me_{tr} might exist in the desert soils in their reduced and/or oxidized form and can participate in the Fenton reaction (5) with their reduced form directly. For example, Fe²⁺ might occur as interlayer species such as the Fe²⁺-aquo complex in the 2:1 clay minerals⁵². Also Fe³⁺ may participate in the Fenton reaction indirectly after its reduction by H₂O₂ (ref. 30) or O₂^{•−} (O₂^{•−} + Me_{tr}ⁿ⁺¹ → Me_{tr}ⁿ + O₂; the sum of this reaction with the Fenton reaction 5 is the Me_{tr}-catalysed Haber–Weiss reaction 6; ref. 12). Therefore, Me_{tr} can convert the weak oxidants H₂O₂ and O₂^{•−} to the highly reactive [•]OH.

We showed that the instability of the Atacama and Mojave Desert soil metal superoxides/peroxides (as H₂PO₄-extracted H₂O₂) in the dark is associated with the production of [•]OH (Fig. 1). The possible involvement of the Fenton reaction mechanism can be implied by the concurrence of the higher (threefold) production of [•]OH in Atacama (Yungay site) over Mojave (+ CIMA site) with the higher concentration of Me_{tr} (four and twofold higher in Cu and Co), respectively (Table 2). H₂O₂ could be destabilized by other factors such as alkaline pH (via the hydrolysis reaction: 2H₂O₂ → 2H₂O + O₂; ref. 53). However, this is not a likely scenario given the stabilizing effect of phosphates and acidic pH on H₂O₂ (ref. 54), with the latter confirmed by the relative stability of a control H₂O₂ solution in 10 mM H₃PO₄ (Fig. 1a). Therefore, the identification of [•]OH in the Atacama aqueous soil extracts (Fig. 1a) could explain the previous observation of the oxidation (to CO₂) of sodium formate and aqueous mixtures of chiral sodium alanine and glucose after incubation for several days with Atacama Desert soil even in the dark, albeit at a slower rate¹. The reactivity of the Atacama Desert soils with organics in the dark may not proceed by direct involvement of ¹O₂, as its lack of charge would hinder its adsorption on the surface of soils. Moreover, non-light-induced abiotic oxidation of organics also may be involved in desert soils because the process has shown that Mn-oxides and Fe-oxides/hydroxides common in desert soils (and in the tested ones, Table 2) could cause oxidation of organics (for example, 17β-estradiol⁵⁵) and aromatic amines⁵⁶. Similarly, perchlorates

(present in both Atacama and Mojave Deserts^{34,35}) could be potential oxidants of soil organics^{57–59}.

The oxidation of soil organics by photogenerated ROS may be a continuous process given that Me_{tr} are ubiquitous in all soils. O_2^- may represent a fraction of the ROS produced in photo-irradiated desert soils, however. Another ROS could be 1O_2 because it is generated—and oxidizes organics—by photo-irradiated minerals such as MgO , Al_2O_3 and SiO_2 (refs 18,19,60), which are common in desert soils and also found in the tested soils (Table 2). Moreover, 1O_2 could be formed directly by reaction of O_2^- with H_2O_2 (refs 61,62), and possibly by the decomposition of light-generated O_2^- on irradiated surface soils¹⁸. In addition, 1O_2 can form O_2^- because it possesses the required one-electron reduction potential (+0.65 V at pH 7.0), while its two-electron reduction could generate H_2O_2 (ref. 43). Therefore, photogeneration of O_2^- from 1O_2 could have been possible under non-aqueous conditions as long as it involves a highly reactive single electron photo-ejected from soil minerals or donated by soil organic photosensitizers.

The present study also showed that O_2^- is photogenerated by desert soils (Fig. 2a). O_2^- is generated at similar levels even by soils prewashed before exposure from polar inorganic and polar/non-polar organic soil constituents, suggesting a mechanism not involving photosensitization and the involvement of perchlorates. These prewashed soils also photogenerated $\cdot OH$ under aqueous conditions (Fig. 3) and at a near 1:1 molar rate ratio with the O_2^- that is generated (in the 1st hour) by sunlight-exposed desiccated soils (Fig. 2a), in agreement with the mechanism for TiO_2 photocatalysis^{15,36}. The same mechanism also could apply for the desert soils (Fig. 4) since they contain transition metal oxides such as TiO_2 and Fe-Ti-oxides (Table 2). Moreover, the photo-catalytic generation of $\cdot OH$ by aqueous desert soils could provide a light-based mechanism for their reactivity with organics. This would involve the photo-catalytic ejection of an electron from metal oxides (to generate O_2^- by dissolved O_2) and the subsequent abstraction of an electron by the resulting h^+_{VB} hole from H_2O or OH^- (resulting also from H_2O via reaction with a bridging-oxygen atom¹⁵). Then, $\cdot OH$ (and H_2O_2 to a lesser degree) could oxidize soil organics to CO_2 and NO_y .

The photogenerated ROS detected in desert soils also may explain the ionizing radiation resistance of certain desert bacteria—notably *Deinococcus radiodurans* and *Chroococcidiopsis*—that can withstand extraordinarily high levels of ionizing radiation⁶³. Radiation resistance is regarded as a proxy for desiccation resistance⁶³. Ionizing radiation also produces reactive oxidants similar to photochemical oxidants⁶⁴. Thus, the ability to withstand photochemical oxidants might explain the resistance of desert bacteria to radiation.

Finally, an extreme example of this soil oxidant chemistry appears to take place on Mars. The oxidative reactivity of the Martian soil as measured by the Viking Biology Experiments (and exhibited on the organics of a certain nutrient by releasing O_2 and CO_2 (refs 65,66)), requires a mix of oxidants in the soil including oxidants capable of destroying organics^{57,67}. Production of O_2^- by the photo-induced transition metal oxide surface- O_2 electron transfer mechanism has been suggested¹⁷. Other alternative potential pathways may involve (i) photogeneration of ROS on mineral substrates (for example, plagioclase) that can generate O_2^- from adsorbed O_2 on TiO_2 and (ii) photoactive on Mars Fe-oxides such as hematite being analogous to TiO_2 in surface catalysis⁴². The source of O_2 needed for the photogeneration of O_2^- in Martian topsoil under an O_2 -depleted atmosphere, however, has not been elucidated. It could be that O_2 might have been released by perchlorate (given its abundance on Mars^{68,69}) on exposure to cosmic radiation. This is supported by the generation of O_2 by perchlorate exposed to gamma rays in a CO_2

atmosphere⁵⁷. Nonetheless, the buildup of soil ROS oxidants on Mars would be less impeded by liquid water than even the driest desert on Earth.

Accumulated metal superoxides and peroxides were detected in soils from the Atacama (hyper-arid) and Mojave (arid) deserts. Moreover, desiccated desert soils photogenerate O_2^- at saturation levels, followed by long-term stabilization by diffusion as soil metal superoxides and peroxides. Desert soils photogenerate $\cdot OH$ under aqueous conditions. The photogeneration of O_2^- by desiccated or aqueous soils may proceed via capture by O_2 of a single electron that is photo-ejected from metal oxides (for example, TiO_2/Fe_2O_3 detected in the tested soils). The resulting h^+_{VB} hole in H_2O -wetted soil metal oxides can, then, abstract a single electron from H_2O or OH^- and generate $\cdot OH$. Moreover, aqueous desert soil metal superoxides/peroxides are converted (by dismutation/hydrolysis, respectively) to H_2O_2 , the observed instability of which in the dark concurs with the generation of $\cdot OH$, possibly via the Fenton reaction due to the presence in these soils of Me_{tr} . The generation of $\cdot OH$, in the dark (via the Fenton reaction) and by photocatalysis could explain the abiotic oxidation of organics by desert soils, with H_2O_2 and O_2^- acting as weak oxidants. Similar ultraviolet-induced processes may take place in the topsoils of Mars.

Methods

Samples and reagents. Full details of sample collection and treatment are available in the Supplementary Methods section, with details of the reagents used.

HE-based soil O_2^- assay. Assay principle and other supporting control experiments are described in full in the Supplementary Methods.

Reagent solutions. *100% alkaline acetonitrile.* It is made by mixing 100% acetonitrile (ACN) with 0.1 M NaOH at a 100:1 ratio. At this NaOH proportion it mixes almost completely as it leaves a small aqueous droplet in the bottom of the tube, resulting in ~99% ACN and higher, the resulting ACN_{alk} solvent is saturated with hydroxyl ions, reaching a stable pH 8–8.5. For the pH measurements a Sentron Argus-type pH Meter was used, equipped with a non-glass Hot-Line electrode (Sentron, The Netherlands).

100 mM CE. It is prepared by dissolving 186 mg dicyclohexano-18-crown-6 ether (CE) in 5 ml ACN_{alk}. Prepare fresh, keep at 4 °C. Caution: accurate pipetting of the reagent is required.

Soil O_2^- ACN_{alk}-CE extraction solutions. Solution ACN_{alk}-CE (0.2 mM) is prepared by mixing 29.94 ml ACN_{alk} with 60 µl 100 mM CE. This standard solution is designated also as ACN_{alk}-CE. ACN_{alk} solutions containing other CE concentrations can be prepared from the 100% ACN_{alk} and 100 mM CE stocks. For example, ACN_{alk}-CE (1 mM) solution is made by mixing 29.7 ml ACN_{alk} with 0.3 ml 100 mM CE. The ACN_{alk}-CE extraction solutions should be prepared fresh, and kept in an airtight and light-protected glass container at 4 °C.

0.5 mM HE. Prepare fresh (and kept at 4 °C, protected from light) by dissolving 1.2 mg HE in 7.5 ml ACN_{alk}-CE (0.2 mM) solution. Caution: accurate pipetting of the reagent is required.

50 mM HCl. Prepare by diluting ×240 (with ddH₂O) the concentrated 37% HCl (or 12 M). Caution: accurate pipetting of the reagent is required.

1 M Tris-base, pH 8.0. Caution: accurate pipetting of the reagent is required.

Protocol. Soil samples were treated as follows: 1 g soil is placed in a 15-ml plastic centrifuge tube (with conical bottom) with 2.5 ml ACN_{alk} or ACN_{alk}-CE (for example, 0.2 mM) and mixed by shaking for 2–3 min at room temperature (RT); to extract O_2^- , and the soil is removed by precipitation (or filtration). The supernatants are diluted appropriately with ACN_{alk}-CE to set the CE concentration in the ACN_{alk} extract to final 0.2 mM and are kept capped in an ice-water bucket.

NOTES: I. Soil metal superoxides can be extracted effectively by an ACN_{alk}-CE solution. Testing various concentrations of CE (for example, 0.2, 1 mM) in the ACN_{alk} extraction solution allows the determination of the optimum CE concentration for solubilizing the maximum quantity of soil metal salts of O_2^- . This can be tested by extracting soil O_2^- with ACN_{alk} mixed with various CE concentrations, to determine a minimum CE concentration above which the extracted O_2^- g⁻¹ soil is constant. II. For extracting soil-adsorbed O_2^- the ACN_{alk} extraction solution does not need the presence of CE and the ACN_{alk} solution can be used alone. However, ACN_{alk} may also extract soil metal superoxides although not as effectively as being in mixture with CE.

The ACN_{alk}-CE supernatants from the preceding step are split in two halves (in two 1.5-ml microcentrifuge tubes), one designated 'sample' (S) and the other

'blank' (B), which are centrifuged at 12,000g for 3 min at RT to remove any soil remnants. Then, 880 μl clear supernatant from each half tube are transferred in new tubes to each of which 80 μl 0.5 mM HE are added (40 μM final in the assay).

NOTES: I. For this step, sample/blank tubes are kept in an ice-water bath. II. If using quartz micro-cuvette holding a sample volume 0.3–0.5 ml, (cuvette dimensions 45 \times 4 \times 4, mm with the Shimadzu RF-1501 spectrofluorometer), the total sample volume required can be minimized to \sim 1 ml (0.45 ml per S and B), which results in halving the volumes of the reagents added in this and in the subsequent two steps.

Thereafter, the following alternative Procedures A and B can be followed:

Procedure A: to the B and S tubes, 20 μl 50 mM CE and 20 μl $\text{ACN}_{\text{alk-CE}}$ (0.2 mM) are added, respectively, followed by the addition in both tubes of 20 μl 50 mM HCl (1 mM H^+ concentration in the final assay mixture) and mixing by inversion up to 1 min. For preparing the assay reagent blanks, in each of the two microcentrifuge tubes 880 μl $\text{ACN}_{\text{alk-CE}}$ (0.2 mM) and 80 μl 0.5 mM HE are added, followed by the addition in one tube of 20 μl 50 mM CE and 20 μl 50 mM HCl (designated $\text{R}_{\text{CE-1 mM}}$) and in the other tube of 20 μl $\text{ACN}_{\text{alk-CE}}$ (0.2 mM) and 20 μl 50 mM HCl (designated $\text{R}_{\text{CE-0.2 mM}}$).

NOTES: I. In the S tube, HE reacts with O_2^- (the reaction requires at least 0.5 mM H^+) and forms the fluorescent product 2-hydroxy ethidium (2-OH- E^+ ; at molar stoichiometric ratio $\text{O}_2^- / 2\text{-OH-}\text{E}^+ = 2/1$) at 0.2 mM CE, while in the B tube, this reaction is inhibited by the inclusion of 1 mM CE. II. For the reaction of HE with O_2^- in 1 mM HCl to take place, the pH of the assay mixture must be acidic (pH 1.5–2). Possible alkalinity of soil may change this pH, therefore, a test of the assay mixture pH must be performed and if needed the final concentration of HCl can be adjusted appropriately to bring the assay pH to 1.5–2. III. This step and the subsequent two steps are performed as soon as possible to minimize the possible oxidation of HE by any extracted soil constituents.

After the 1-min incubation period, the assay mixtures in the S, B, $\text{R}_{\text{CE-1 mM}}$ and $\text{R}_{\text{CE-0.2 mM}}$ tubes are mixed with 10 μl 1 M Tris by brief vortexing (to adjust the assay mixture pH to \sim 8), centrifuged at 12,000g for 1 min and the resulting supernatants are collected for fluorescence measurement.

The fluorescence units (FUs) of the S, B, $\text{R}_{\text{CE-0.2 mM}}$ and $\text{R}_{\text{CE-1 mM}}$ supernatants are measured at ex/em 505/580 nm (designated FU_S , FU_B , $\text{FU}_{\text{R}_{\text{CE-0.2 mM}}}$ and $\text{FU}_{\text{R}_{\text{CE-1 mM}}}$, respectively). From these FU, the net FU of 2-OH- E^+ is calculated from the following formula: net $\text{FU}_{2\text{-OH-}\text{E}^+} = \text{FU}_\text{S} - \text{FU}_\text{B} - (\text{FU}_{\text{R}_{\text{CE-0.2 mM}}} - \text{FU}_{\text{R}_{\text{CE-1 mM}}})$.

NOTES: I. To verify that the net $\text{FU}_{2\text{-OH-}\text{E}^+}$ corresponds to the concentration of the extracted O_2^- , various dilutions of the $\text{ACN}_{\text{alk-CE}}$ supernatants (derived in the first two steps of the Assay Protocol) should be tested (as in this and the previous two steps in Procedure A) and only those dilutions resulting in proportional $\text{FU}_{2\text{-OH-}\text{E}^+}$ values will be used for determining the final average $\text{FU}_{2\text{-OH-}\text{E}^+}$ value. II. The $\text{FU}_{\text{R}_{\text{CE-0.2 mM}}}$ and $\text{FU}_{\text{R}_{\text{CE-1 mM}}}$ values can be kept as low as possible by setting the HE final concentration in the assay (see second step in the Assay Protocol) at low levels (for example, 20–40 μM HE), given that O_2^- is quite stable in the ACN_{alk} extraction solvent. The $\text{FU}_{\text{R}_{\text{CE-0.2 mM}}} - \text{FU}_{\text{R}_{\text{CE-1 mM}}}$ value is in the order of 50 FU. Much higher values suggest an excessive autooxidation of HE, and a fresh HE stock solution (see Assay Reagent Solutions) should be used. III. In case $\text{FU}_\text{S} < \text{FU}_\text{B}$, the soil extract may contain a soil constituent, which in the presence of 1 mM CE (in tube B) oxidizes HE to E^+ . In this case, the alternative Procedure B is followed.

Procedure B: to the B and S tubes, 40 and 20 μl $\text{ACN}_{\text{alk-CE}}$ (0.2 mM) are added, respectively, followed by the addition in the S tube of 20 μl 50 mM HCl (1 mM H^+ concentration in the final assay mixture) and mixing by inversion up to 1 min. For preparing the assay reagent blanks, in each of the two microcentrifuge tubes 880 μl $\text{ACN}_{\text{alk-CE}}$ (0.2 mM) and 80 μl 0.5 mM HE are added, followed by the addition in one tube of 20 μl $\text{ACN}_{\text{alk-CE}}$ (0.2 mM) and 20 μl 50 mM HCl (designated $\text{R}_{\text{HCl-1 mM}}$) and in the other tube of 40 μl $\text{ACN}_{\text{alk-CE}}$ (0.2 mM) (designated $\text{R}_{\text{HCl-0 mM}}$).

NOTES: I. In the S tube, HE reacts with O_2^- (the reaction requires at least 0.5 mM H^+) and forms the fluorescent product 2-OH- E^+ (at 0.2 mM CE), while in the B tube, this reaction does not take place (also in the presence of 0.2 mM CE) because HCl is absent. II. For the reaction of HE with O_2^- in 1 mM HCl to take place, the pH of the assay mixture must be acidic (pH 1.5–2). Possible alkalinity of soil may change this pH, therefore, a test of the assay mixture pH must be performed, and if needed the final concentration of HCl can be adjusted appropriately to bring the assay pH to 1.5–2. III. This step and the subsequent two steps are performed as soon as possible to minimize the possible oxidation of HE by any co-extracted soil constituents.

After the 1-min incubation period, the assay mixtures in the S, B, $\text{R}_{\text{HCl-1 mM}}$ and $\text{R}_{\text{HCl-0 mM}}$ tubes are mixed with 10 μl 1 M Tris by brief vortexing (to adjust the assay mixture pH to 7–8), centrifuged at 12,000g for 1 min and the resulting supernatants are collected for fluorescence measurement.

The FU of the S, B, $\text{R}_{\text{HCl-0 mM}}$ and $\text{R}_{\text{HCl-1 mM}}$ supernatants are measured at ex/em 505/580 nm (designated FU_S , FU_B , $\text{FU}_{\text{R}_{\text{HCl-0 mM}}}$ and $\text{FU}_{\text{R}_{\text{HCl-1 mM}}}$, respectively). From these FU, the net FU of 2-OH- E^+ is calculated from the following formula: net $\text{FU}_{2\text{-OH-}\text{E}^+} = \text{FU}_\text{S} - \text{FU}_\text{B} - (\text{FU}_{\text{R}_{\text{HCl-1 mM}}} - \text{FU}_{\text{R}_{\text{HCl-0 mM}}})$.

NOTES: I. To verify that net $\text{FU}_{2\text{-OH-}\text{E}^+}$ corresponds to the concentration of the extracted O_2^- , various dilutions of the $\text{ACN}_{\text{alk-CE}}$ supernatants (derived as in the first two steps of the Assay Protocol) should be tested (as in this and the previous

two steps in Procedure B) and only those dilutions resulting in proportional $\text{FU}_{2\text{-OH-}\text{E}^+}$ values will be used for determining the final average $\text{FU}_{2\text{-OH-}\text{E}^+}$ value. II. The $\text{FU}_{\text{R}_{\text{CE-0.2 mM}}}$ and $\text{FU}_{\text{R}_{\text{CE-1 mM}}}$ values can be kept as low as possible by setting the HE final concentration in the assay (see second step in the Assay Protocol) at low levels (for example, 20–40 μM HE). The $\text{FU}_{\text{R}_{\text{HCl-1 mM}}} - \text{FU}_{\text{R}_{\text{HCl-0 mM}}}$ value should be in the order of 100 FU. Much higher values suggest an excessive autooxidation of HE, and a fresh HE stock solution (see Assay Reagent Solutions) should be used.

To convert the net $\text{FU}_{2\text{-OH-}\text{E}^+}$ value to the concentration of 2-OH- E^+ (and subsequently of O_2^-) in the assay mixture volume (1 ml, in this case), the spectrofluorometer in use must be calibrated with known concentrations of 2-OH- E^+ by determining the fluorescence extinction coefficient of 2-OH- E^+ ($\text{FEC}_{2\text{-OH-}\text{E}^+}$, expressed in FU per $1 \mu\text{M}^{-1}$ 2-OH- E^+) as follows.

The $\text{FEC}_{2\text{-OH-}\text{E}^+}$ is determined in final 97% ACN (same as the ACN final concentration in the assay reaction mixture) for the spectrofluorometer (set at high sensitivity) and quartz cuvette in use in this study, as follows: from a synthetic 2-OH- E^+ stock solution (see Supplementary Methods) of known concentration, 1 μM 2-OH- E^+ in 1 ml ACN_{alk} (or 1 ml $\text{ACN}_{\text{alk-CE}}$ extraction solution) is prepared in a 1.5-ml microcentrifuge tube, to that 2 μl ddH₂O and 30 μl 0.33 M Tris solution are added, and vortexed, and centrifuged at 12,000g for 1 min. Similarly is treated a reagent blank, which is prepared with 1 ml ACN_{alk} (or 1 ml $\text{ACN}_{\text{alk-CE}}$ extraction solution), containing 2 μl ddH₂O and 30 μl 0.33 M Tris solution. $\text{FEC}_{2\text{-OH-}\text{E}^+}$ is determined by measuring the FU value of the clear 1 μM 2-OH- E^+ supernatant (at ex/em 505/580 nm) and subtracting from this value the FU of the clear supernatant of the blank.

Having determined $\text{FEC}_{2\text{-OH-}\text{E}^+}$ in the preceding step, and given the molar stoichiometric ratio $\text{O}_2^- / 2\text{-OH-}\text{E}^+ = 2/1$, the net $\text{FU}_{2\text{-OH-}\text{E}^+}$ (determined three steps before) is converted to a μM concentration of 2-OH- E^+ (in the assay mixture volume) and then to μM O_2^- by the formula (see derivation in Supplementary Methods):

$$\text{O}_2^- (\mu\text{M}) = 2 \times [2\text{-OH-}\text{E}^+ (\text{in } \mu\text{M})] = 2 \times \left(\text{FU}_{2\text{-OH-}\text{E}^+} / \text{FEC}_{\text{ex/em 505/580 nm}} \right) = 2 \times \text{FU} / 1300$$

Finally, the μM O_2^- (extracted from a known soil quantity) are converted to nmoles $\text{O}_2^- \text{g}^{-1}$ soil.

Assay sensitivity. Applying the protocol on 1 g soil, extracted in 1 ml $\text{ACN}_{\text{alk-CE}}$ solution by filtration (to recover a \sim 1.0 ml $\text{ACN}_{\text{alk-CE}}$ extract), with an assay reaction volume 0.5 ml (containing 0.44 ml $\text{ACN}_{\text{alk-CE}}$ extract) and a minimum net $\text{FU}_{2\text{-OH-}\text{E}^+} = 200$, the theoretical assay sensitivity (using the above formula) is $= 200 \times 2/1300 = \sim 0.3 \mu\text{M}$ O_2^- (in the assay reaction mixture, or 0.34 nmoles in 1.0 ml $\text{ACN}_{\text{alk-CE}}$ extract, or 0.34 nmoles g^{-1} soil).

SOD-inhibited reduction of cyt. c-based soil O_2^- assay. Protocol. Soil samples were mixed with a minimum 0.3 ml O_2^- -degassed $\text{ACN}_{\text{alk-CE}}$ (0.2 mM) per gram of soil by shaking for 2–3 min at RT. This proportion achieves the maximum concentration of O_2^- extracted in a minimum solvent volume. Then, \sim 0.5 g batches of this soil/ $\text{ACN}_{\text{alk-CE}}$ slurry were placed in centrifuge tube filters fitted to a 1.5-ml microcentrifuge collection tube, centrifuged at 15,000g for 5 min and the $\text{O}_2^- / \text{ACN}_{\text{alk-CE}}$ eluents of all the batches were combined and used in the following step.

NOTE: In this step and in subsequent steps, all the reagents used should be O_2^- -degassed as in two steps before.

Having established the molar stoichiometric ratio 1:1 of O_2^- to cyt. c_{red} up to a final 40% $\text{ACN}_{\text{alk-CE}}$ (see Supplementary Methods), the maximum $\text{ACN}_{\text{alk-CE}}$ solvent volume for the recovery of O_2^- from any soil sample is 0.4 ml. This volume is sufficient for the control if \sim 0.5-volume capacity cuvettes are used. Given that the minimum proportion of $\text{ACN}_{\text{alk-CE}}$ extraction volume/soil weight is \sim 0.3 ml per 1 g, the maximum amount of soil that this assay can extract for measuring accurately the concentration of O_2^- in a 0.4 ml extract is 1.3 g. Therefore, 1.3-g soil samples were used extracted in 0.4 ml $\text{ACN}_{\text{alk-CE}}$, and were diluted with 100% $\text{ACN}_{\text{alk-CE}}$ to 0.8 ml (unless a smaller than 1-ml spectrophotometer cuvette is used). A 0.4 ml portion of the clear $\text{ACN}_{\text{alk-CE-}\text{O}_2^-}$ extract (after centrifugation at 15,000g for 5 min) was mixed with 0.6 ml 50 mM phosphate buffer, pH 7.8, containing 26.7 μM cyt. c_{ox} (final 16 μM). Its absorbance was measured at 550 nm against a reagent blank (0.4 ml $\text{ACN}_{\text{alk-CE}}$ plus 0.6 ml 50 mM phosphate buffer, pH 7.8) and also against the following SOD blank: It consists of the remaining 0.4-ml portion of the $\text{ACN}_{\text{alk-CE}}$ extract, mixed with 0.6 ml 50 mM phosphate buffer, pH 7.8, containing 26.7 μM cyt. c_{ox} and 3.3 units SOD (or SOD added before the addition of cyt. c_{ox}). If O_2^- is present in the 0.4 ml $\text{ACN}_{\text{alk-CE}}$ extract the assay will identify it from the SOD-inhibited reduction of cyt. c_{ox} . Competing with cyt. c_{ox} , SOD will reduce or eliminate the concentration of O_2^- by dismutation. This blank also quantifies possible soil contaminants that may cause chemical reduction of cyt. c_{ox} and/or absorb at 550 nm. Then, the $\Delta A_{550 \text{ nm}}$ (absorbance of the sample minus absorbance of the SOD blank) is converted nmoles of cyt. c_{red} which correspond to equimolar O_2^- derived from the standard curve of cyt. c_{red} versus O_2^- concentration (see Supplementary Methods). The sensitivity of the assay is \sim 0.5 nmoles O_2^- (or 0.5 μM in the $\text{ACN}_{\text{alk-CE}}$ /phosphate buffer assay mixture).

NOTE: The 0.4 ml of the $\text{ACN}_{\text{alk}}\text{-CE-O}_2^-$ soil extract should be rapidly mixed with the 0.6-ml phosphate-buffered cyt. c_{ox} in the spectrophotometer cuvette and its peak absorbance immediately measured as it rapidly decreases due to the reoxidation of cyt. c_{red} .

Assay for soil total metal superoxides/peroxides and Fe^{3+} . *Reagent solutions.* FOX (Ferrous Oxidation in Xylenol orange) assay reagents. In a plastic vial (glass vials may leak Fe^{3+}), 3.644 g sorbitol (final 2 M, and in assay reaction 0.1 M) and 15.2 mg xylenol orange are dissolved (for about 30 min) in 7.6 ml 0.66 M HClO_4 (final 0.5 M, and in assay reaction 25 mM). Then, any non-dissolved matter is removed by centrifugation (or by filtering), the resulting supernatant is split in two halves (5 ml each), and one half is the FOX- Fe^{2+} reagent. To the other half, 7.9 mg ferrous ammonium sulfate are dissolved, resulting in the FOX + Fe^{2+} reagent. Both the reagents are prepared fresh.

0.1 M EDTA stock. It is prepared in ddH_2O . EDTA is a Fe^{3+} chelator, and is used here as blank for the estimation of soil Fe^{3+} .

Standard curves. H_2O_2 (0–2 μM) standard curve. It is made with a 4 μM H_2O_2 solution (in 10 mM phosphate buffer, pH 6.5) prepared from a 5 mM H_2O_2 working stock, which is made from the concentrated 30% H_2O_2 using the H_2O_2 molar extinction coefficient at 240 nm ($\epsilon_{240} = 43.6 \text{ M}^{-1} \text{ cm}^{-1}$). The reagents are mixed as presented in the following box:

Tube numbers (μM H_2O_2 , or nmol H_2O_2 in 1 ml assay reaction). Reagents in μl	0	0.2	0.4	0.6	0.8	1	1.2	1.4	1.6	2
4 μM H_2O_2	0	50	100	150	200	250	300	350	400	500
10 mM phosphate buffer, pH 6.5	950	900	850	800	750	700	650	600	550	450
FOX + Fe^{2+} reagent										50 μl in each tube

Each tube is then incubated for 30 min at RT after which the absorbance at 560 nm ($A_{560 \text{ nm}}$) of each of the assay reaction mixtures in tubes 0–2 is measured. The net $A_{560 \text{ nm}}$ value of tubes 0.2–2 is calculated by subtracting from their $A_{560 \text{ nm}}$ value the $A_{560 \text{ nm}}$ value of tube 0 (the blank). Then, the standard curve is drawn by plotting the 0–2 μM (or nmoles) H_2O_2 against their corresponding net $A_{560 \text{ nm}}$ values.

NOTE: With 10 mM phosphate, pH 6.5, as H_2O_2 /sample solvent, the final 25 mM perchloric acid in the assay achieves assay reaction pH ~ 1.8 . At these conditions, the assay achieves its highest, for H_2O_2 , molar extinction coefficient $\sim 250,000 \text{ M}^{-1} \text{ cm}^{-1}$. With unbuffered samples (that is, in H_2O), the final concentration of perchloric acid in the assay should be 15.5 mM (in H^+), which corresponds to the optimal assay pH 1.8.

Fe^{3+} (0–12 μM) standard curve. It is made from a 20 μM Fe^{3+} stock solution (in 10 mM phosphate buffer, pH 6.5). The reagents are mixed as presented in the following box:

Tube numbers (μM Fe^{3+} , or nmol Fe^{3+} in 1 ml assay reaction). Reagents in μl	0	1	2	4	6	8	10	12
20 μM Fe^{3+} (in 10 mM phosphate buffer, pH 6.5)	0	50	100	200	300	400	500	600
10 mM phosphate buffer, pH 6.5	950	900	850	750	650	550	450	350
FOX- Fe^{2+} reagent								50 in each tube

Each tube is then incubated for 30 min at RT after which the absorbance at 560 nm ($A_{560 \text{ nm}}$) of each of the assay reaction mixtures in tubes 0–12 is measured. The net $A_{560 \text{ nm}}$ value of tubes 1–12 is calculated by subtracting from their $A_{560 \text{ nm}}$ value the $A_{560 \text{ nm}}$ value of tube 0 (the blank). Then, the standard curve is plotted as 0–12 μM (or nmoles) Fe^{3+} against their corresponding net $A_{560 \text{ nm}}$ values.

Protocol. Soil samples were treated as follows: 1 g soil (placed in a capped 15-ml plastic centrifuge tube) was extracted in (for example, 1–4 ml) 10 mM H_3PO_4 for 2 min by gentle inversion and the soil extract was collected by centrifugation at 5,000g for 5 min.

NOTE: Extraction of the Mojave and Atacama soil samples with 10 mM H_3PO_4 resulted in pH ~ 6.5 of the soil H_2O_2 extract.

The soil extract (its pH is adjusted to ~ 6.5 with 0.1 M NaOH/HCl if needed) was treated with the assay reagents (in 1.5-ml microcentrifuge tubes) shown as presented in the following box:

Sample treatments (STs) and reagent blanks (RBs): Reagents in μl	ST1	ST2	ST3	ST4	RB1	RB2
Soil extract (or appropriate dilutions in 10 mM phosphate buffer, pH 6.5)	935	935	935	935	—	—
10 mM phosphate buffer, pH 6.5	15	—	15	—	950	935
3 KU ml^{-1} CAT (in 10 mM phosphate buffer, pH 6.5)	—	15	—	—	—	15
5-min incubation	No	Yes	No	No	No	Yes
0.1 M EDTA	—	—	—	15	—	—
1-min incubation	No	No	No	Yes	No	No
FOX + Fe^{2+} reagent	50	50	—	—	50	50
FOX- Fe^{2+} reagent	—	—	50	50	—	—

After mixing, the ST1, ST2, ST3, ST4, RB1 and RB2 tubes are incubated for 30 min at RT. NOTE: For higher accuracy, ST1, ST2, ST3 and ST4 mixtures are preferably made each in triplicates from three different soil extract dilutions, while RB1 and RB2 are made in triplicates.

The corresponding A_{ST1} , A_{ST2} , A_{ST3} , A_{ST4} , A_{RB1} and A_{RB2} absorbance values are recorded at 560 nm, and their triplicate averages are then entered in the following equations to calculate the corresponding net $A_{560 \text{ nm}}$ for soil H_2O_2 and Fe^{3+} , which are then converted to H_2O_2 and Fe^{3+} concentrations (from the corresponding standard curves), expressed per g soil:

$$\text{Soil } \text{H}_2\text{O}_2 \text{ net } A_{560 \text{ nm}} = A_{\text{ST1}} - A_{\text{ST2}} + (A_{\text{RB2}} - A_{\text{RB1}})$$

$$\text{Soil } \text{Fe}^{3+} \text{ net } A_{560 \text{ nm}} = A_{\text{ST3}} - A_{\text{ST4}}$$

Instability of aqueous desert soil superoxides/peroxides. To test whether the instability of soil H_2O_2 extracts (from total metal peroxides) during various incubation intervals concurs with the generation of $\cdot\text{OH}$ radicals, these were trapped in the H_2O_2 extracts by TPA and the resulting specific fluorescent product 2-hydroxyl terephthalate (HTPA) was isolated and quantified by the following procedure developed for this study.

Procedure: Soil H_2O_2 extracts were analysed for stability and $\cdot\text{OH}$ generation versus extract incubation time (0–48 h) in the absence (A) and presence (B) of the extracted soil. Specifically, H_2O_2 was extracted from two 1-g soil samples (per incubation time interval) after each was mixed with 4 ml 10 mM H_3PO_4 for 5 min at RT, followed by centrifugation at 4,200g for 3 min. The H_2O_2 extract in the isolated supernatant (in the absence of the soil precipitate) was kept for treatment A and that in the upper aqueous phase (in the presence of the soil precipitate) was kept for treatment B. Stability of H_2O_2 in extract samples from treatment A was measured as the remaining H_2O_2 concentration after certain incubation time intervals (up to 48 h) at RT, using as control a solution of 2 μM H_2O_2 in 10 mM H_3PO_4 (made from the 30% H_2O_2 , the preparation of which is described in the H_2O_2 standard curve presented in the Methods section 'Assay for soil total metal superoxides/peroxides and Fe^{3+} '). The concentration of H_2O_2 was measured as described in the Methods section 'Assay for soil total superoxides/peroxides and Fe^{3+} '. More experimental details are also presented in the legend of Fig. 1. To measure the generation of $\cdot\text{OH}$ in the extracts of treatments A and B, they were both brought to 2 mM TPA (from a 100 mM TPA stock made by dissolving 115 mg TPA in 1.4 ml 1 M NaOH and then mixing with 1.4 ml 50 mM phosphate buffer, pH 7.4, readjusted with 1 M HCl and ddH_2O to final 7 ml) and incubated at RT in the dark for the selected time intervals. As control, corresponding soil extracts were also incubated with 100 mM DMSO, an $\cdot\text{OH}$ scavenger. After each incubation period, 0.9 ml of the soil extracts for treatments A and B were mixed with 9 μl 10 M NaOH (to ensure deprotonation of HTPA) and washed with an equal volume ethyl acetate-ethanol (2:1) by vortexing, followed by centrifugation at 4,200g for 5 min. The resulting bottom aqueous phase (~ 1.2 ml) was acidified by 25 μl 10 M HCl (to protonate HTPA) and HTPA (and TPA) was extracted (by vortexing) with two 0.9-ml ethyl acetate washes, followed by centrifugation for 5 min at 4,200g. The combined 1.8 ml ethyl acetate phase was washed with 1.8 ml 0.1 M HCl and evaporated in a rotary vacuum concentrator. The resulting solid precipitate was dissolved in 15 mM KOH (at a minimum volume for example, ~ 0.1 ml) and adjusted to pH 7 (with 0.2 M KH_2PO_4 , pH 7) for high-performance liquid chromatography (HPLC) analysis. Samples (10 μl) were injected into an Shimadzu HPLC Prominence UFLC system, consisting of a solvent delivery system (model LC-20AD), a sample manual injector (Rheodyne 7725i), an on-line degasser (DGU-20A5), a reverse-phase C18 column (Waters Nova-Pak C18, 60 Å, 4 μm , 3.9 \times 150 mm) and a fluorescent detector (RF-20Axs) set at ex/em 311/425 nm. The mobile phase, consisting of 50 mM KH_2PO_4 in 30% methanol, pH 3.2 (an alternative mobile phase is 0.2 M KH_2PO_4 , pH 4.37, containing 2% of KCl^{70}), was passed through the column at a flow rate 0.8 ml min^{-1} and the sample was eluted for a total of 20 min. HTPA in samples was identified and quantified by HPLC-fluorescence (eluted as a peak at ~ 14 min) against pure HTPA (article Fig. 1b), which was synthesized as reported in the Supplementary Methods. HTPA was also identified by mass spectroscopy using an Agilent 1260 Infinity HPLC-MS system equipped with a binary pump, an auto-sampler and a micro-column Zorbax Extend-

C18 600Bar 2.1 × 50 mm, 1.8 μM, connected on line with an Agilent 6538 UHD Accurate-Mass Q-TOF LC/MS detector, operated in negative (ESI⁻) electrospray ionization mode. Samples (10 μl) were eluted under linear gradient conditions (at a flow rate 0.3 ml min⁻¹ for 10 min) at RT, by an increasing 100% ACN (solvent A) and a decreasing 50 mM KH₂PO₄, pH 3.2, 30% MeOH (solvent B) mobile solvent phase. The microcolumn was initially washed with the A and subsequently equilibrated with the solvent B. HTPA (eluted as a peak at ~1.5 min) was identified as giving, for the parent ion, *m/z* with highest peak at *M*-1 = 181.01437 (versus the theoretical 181.01425), and a fragmentation product at *M*-1 = 137.02442 (expected from the fragmentation, at CE 20 eV, of one carboxyl group from HTPA).

Soil O₂⁻ generation by sunlight and ultraviolet-C. Procedure: Soils (~1 g), untreated or washed (to remove any soluble inorganics/organics and polar/hydrophobic organics by vortexing (and intermittent centrifugation at 4,200g for 5 min) with 2 × 10 ml 0.1 M HCl, 1 × 10 ml ddH₂O, 2 × 10 ml 0.1 M NaOH, 3 × 10 ml ddH₂O, 2 × 5 ml ddH₂O plus 5 ml ethyl acetate:ethanol (2:1), 1 × 10 ml 25% ethanol, and finally dried at 150 °C for 1 h) were spread as a thin layer on aluminum foil and exposed to natural sunlight (at 800–1,000 W m⁻², in a July day, from 10:00 to 16:00 hours and at an average 45 °C); unexposed were used as control. The relative humidity at 10:00 hours was ~15% and reached a minimum ~5% during the exposure period. Soils were also exposed to ultraviolet C radiation (using a germicidal lamp with flux density 30 μW cm⁻² set at a close distance of 10 cm) at relative humidity 10–25% and at an average 40 °C. After irradiation, soils were extracted for O₂⁻ (as in the Methods section 'HE-based soil O₂⁻ assay') and measured by the aforementioned HE-based and SOD-inhibited reduction of cyt. *c*-based soil O₂⁻ assays. Irradiated soils were also extracted for total superoxides/peroxides and the resulting H₂O₂ extract was measured as in the Methods section 'Assay for soil total metal superoxides/peroxides and Fe³⁺'.

Photo-generation of ·OH by aqueous desert soils. Procedure: Soil samples were extensively washed as in the Methods section 'Soil O₂⁻ generation by sunlight and ultraviolet C' to remove any soluble inorganic/organic and polar/hydrophobic organic soil constituents, which may affect the rate of photogeneration of ·OH. Washed soil samples (0.2 g) were placed in capped small plastic Petri plates (inner diameter 5 cm), mixed with 10 ml ddH₂O and spread as an even thin layer on the plate bottom with a small glass rod. Then, 50 μl from the 100 mM TPA stock solution (made in 400 mM NaOH) was added. This resulted in final 0.5 mM TPA and 1 mM NaOH (due to its partial neutralization by the 1 mM carboxyl groups of 0.5 mM TPA), which were set as an optimal for the ·OH-TPA assay in a previous study using illuminated TiO₂ films^{37,38}. Samples were exposed to light irradiation 180 W m⁻² (at 400–800 nm, emitted by two halogen lamps, type R7s J118 tube linear 500W/230V ~9000 Lumens per m² each, both covered with glass and ultraviolet and infrared cutoff filters and set at 50 cm above the soil plates) or higher (adding more lamps) and for up to 10 h (at RT). The following light-exposed controls were used: (a) soil samples mixed with 10 ml 1 mM NaOH (for soil interference), (b) 10 ml 1 mM NaOH (for aqueous phase treatment interference), (c) 10 ml 0.5 mM TPA and 2 mM NaOH (for TPA interference) ± 100 mM DMSO (·OH scavenger), (d) 10 ml 1 μM H₂O₂ in 0.5 mM TPA and 2 mM NaOH (to test possible photolysis of H₂O₂ to ·OH; both can be products of, for example, TiO₂ photocatalysis³⁸, given that H₂O₂ can be generated directly or indirectly, for example, via dismutation, from O₂⁻) and (e) 10 ml suspension of 1.6 mg TiO₂ (or 20 μM TiO₂) in 0.5 mM TPA and 2 mM NaOH (for testing the employed assay to detect ·OH photo-generation and by simulating a photocatalysis mechanism with TiO₂). The amount of TiO₂ used is equivalent to the average concentration (w%) in the 0.2 g soils from Atacama Yungay and Mojave + CIMA sites (Table 2). Exposure of the soil samples to ultraviolet C irradiation was not used because the control (c) produced ·OH, possibly because the ultraviolet C lamp may also emit near the absorbance of water (186 nm) and, thus, photo-dissociate it to ·OH. Aqueous samples (1 ml) were drawn from the plates at certain time intervals, centrifuged at 16,000g for 5 min at RT, acidified with final 0.1 M HCl, extracted × 2 with 1 ml ethyl acetate (by vortexing and subsequent centrifugation at 4,000g) and dried by a centrifugal vacuum concentrator at 50 °C. The isolated HTPA solid precipitate in soil and control samples was dissolved in 0.1 ml 20 mM NaOH (its moles are × 2 those of the total carboxy groups of added TPA) and neutralized by 0.2 ml 150 mM K-phosphate buffer, pH 7.4. The solubilized HTPA was quantified by HPLC-fluorescence (as in the Methods section 'Instability of aqueous desert soil superoxides/peroxides'), and, in routine HTPA quantifications by measuring the fluorescence difference emission spectra (recorded at the excitation wavelength 311 nm) of samples minus those of appropriate controls as follows: Starting with the determination of the emission spectra of controls (a) and (b), they were found identical (indicating that washed soil did not interfere) and lower in FUs than of the control (c) spectrum, which shows that both the controls were part of the control (c). Therefore, the emission spectrum of latter control was subtracted from the soil sample emission spectra taken at different exposure time periods, to estimate the corresponding net emission spectra due to HTPA present in the samples. These HTPA spectra were identified by comparing their shape and peak at 425 nm with the spectra of pure HTPA (synthesized as in the Methods section 'Instability of aqueous desert soil superoxides/peroxides'), and with the known emission spectra of HTPA, which are

stable at a pH range 5.5–9.5 (ref. 70). Similarly, the control (c) emission spectrum was subtracted from the emission spectra of controls (d) and (e) to identify the formation of HTPA due to H₂O₂ and TiO₂, respectively. The net FU emission peak (at 425 nm with excitation at 311 nm) in the difference spectra was, then, converted to HTPA concentration by a spectrofluorometer (Shimadzu RF-1501) calibrated with 1 μM pure HTPA; it emits ~300 FU at the spectrofluorometer's low sensitivity setting (or 15,000 FU at the high-sensitivity setting). Additional data analysis is presented in the corresponding section of the Supplementary Methods.

Mineralogical and geochemical analysis of soils. Procedure: The bulk mineralogy of the samples was determined by X-ray diffraction on the D8 Advance diffractometer (Bruker AXS) equipped with a LynxEye strip silicon detector, using Ni-filtered CuKα radiation, an applied voltage 35 kV and a 35 mA current, and 0.298° divergence and antiscatter slits. The random powder mounts of samples were scanned from 2 to 70° 2θ with a scanning step of 0.015° 2θ and with 18.7-s count time per step. Powder diffraction data were collected at RT. Results were confirmed with synchrotron X-ray high-resolution powder diffraction measurements. The samples were loaded into 1.0 mm-diameter glass capillaries. Powder diffraction data (for Atacama Yungay and site 1, and Mojave + CIMA basalt rock samples) were collected at RT (295 K) on the undulator beamline ID31 at the ESRF (European Synchrotron Radiation Facility) in Grenoble, France. The parallel beam geometry instrument is equipped with nine Si(111) analyser crystals and provides data with very high angular resolution, with a minimum instrumental contribution to the full-width half-maximum around 0.003°. High speed spinning of the sample was applied to ensure sufficient powder averaging. The nine detector modules (separated by ~2°) were scanned over a 40° 2θ range, at a wavelength of 0.400054(15) Å, using an incident beam size of 2.0 mm (2.0 mm (horizontally) × 1.0 mm (vertically)). The clay fraction (<2 μm) was separated by settling and dried on glass slides at RT. Clay minerals were identified from air dried slides and after ethylene glycol solvation at 60 °C overnight to ensure maximum saturation. X-ray diffraction analysis was performed from 2 to 35° 2θ with the Bruker D8 Advance diffractometer, using the same divergence and antiscatter slits, and a step size of 0.019° 2θ, with 47.7-s count time per step. Chemical composition of minerals was examined with a JEOL 6300 Scanning Electron Microscope equipped with an Oxford Link Energy Dispersive Spectrometer (EDS; Oxford Instruments). Semi-quantitative analyses of minerals were performed on sample powders mounted directly on glass slides and coated with carbon. The chemical composition of the minerals was determined using natural and synthetic standards and 20 kV accelerating voltage with 10 nA beam current. Back-scattered electron images were used to identify any heavy minerals present. The concentrations of major and trace elements in bulk samples (from Atacama sites, Mojave sites and control site) were determined with Energy Dispersive X-ray Fluorescence Spectroscopy (EDS-XRF, S2 Ranger, Bruker). The samples were fused using a flux:sample powder ratio of 5:1 and were casted in dies forming glass beads. Li-tetraborate was used as flux. Additional data analyses can be found in the corresponding section of the Supplementary Methods.

References

1. Navarro-Gonzalez, R *et al.* Mars-like soils in the Atacama desert, Chile, and the dry limit of microbial life. *Science* **302**, 1018–1021 (2003).
2. Quinn, R. C., Ehrenfreund, P., Grunthaner, F. J., Taylor, C. L. & Zent, A. P. Decomposition of aqueous organic compounds in the Atacama Desert and in Martian soils. *J. Geophys. Res.* **112**, G04S18 (2007).
3. McCalley, C. K. & Sparks, J. P. Abiotic gas formation drives nitrogen loss from a desert ecosystem. *Science* **326**, 837–840 (2009).
4. Austin, A. T. & Vivanco, L. Plant litter decomposition in a semi-arid ecosystem controlled by photodegradation. *Nature* **442**, 555–558 (2006).
5. Gohre, K. & Miller, G. C. Singlet oxygen generation on soil surfaces. *J. Agric. Food Chem.* **31**, 1104–1108 (1983).
6. Katagi, T. Photodegradation of 3-phenoxybenzoic acid in water and on solid surfaces. *J. Agric. Food Chem.* **40**, 1269–1274 (1992).
7. Misra, B., Graebing, P. W. & Chib, J. S. Photodegradation of chloramben on a soil surface: a laboratory-controlled study. *J. Agric. Food Chem.* **45**, 1464–1467 (1997).
8. Hebert, V. R. & Miller, G. C. Depth dependence of direct and indirect photolysis on soil surfaces. *J. Agric. Food Chem.* **38**, 913–918 (1990).
9. Frank, M. P., Graebing, P. & Chib, J. S. Effect of soil moisture and sample depth on pesticide photolysis. *J. Agric. Food Chem.* **50**, 2607–2614 (2002).
10. Katagi, K. Photodegradation of pesticides on plant and soil surfaces. *Rev. Environ. Contam. Toxicol.* **182**, 1–195 (2004).
11. Suzuki, Y., Lopez, A., Ponte, M., Fujisawa, T., Ruzo, L. O. & Katagi, T. Photoinduced oxidation of the insecticide phenothrin on soil surfaces. *J. Agric. Food Chem.* **59**, 10182–10190 (2011).
12. Halliwell, B. & Gutteridge, C. M. J. *Free Radicals in Biology and Medicine* 3rd edn (Oxford Univ. Press, 1999).
13. Lunsford, J. H. ESR of adsorbed oxygen species. *Catal. Rev.* **8**, 135–157 (1973).
14. Che, M. & Tench, A. J. Characterization and reactivity of molecular oxygen species on oxide surfaces. *Adv. Catal.* **32**, 1–148 (1983).

15. Linsebigler, A. L., Lu, G & Yates, J. T. Photocatalysis on TiO₂ surfaces: principles, mechanisms, and selected results. *Chem. Rev.* **95**, 735–758 (1995).
16. Ito, T., Kato, M., Toi, K., Shirakawa, T., Ikemoto, I & Tokuda, T. Oxygen species adsorbed on ultraviolet-irradiated magnesium oxide. *J. Chem. Soc., Faraday Trans. 1* **81**, 2835–2844 (1985).
17. Yen, A. S., Kim, S. S., Hecht, M. H., Frant, M. S. & Murray, B. Evidence that the reactivity of the Martian soil is due to superoxide ions. *Science* **289**, 1909–1912 (2000).
18. Gohre, K., Scholl, R. & Miller, G. C. Singlet oxygen reactions on irradiated soil surfaces. *Environ. Sci. Technol.* **20**, 934–938 (1986).
19. Gohre, K. & Miller, G. C. Photochemical generation of singlet oxygen on non-transition-metal oxide surfaces. *J. Chem. Soc., Faraday Trans. 1* **81**, 793–800 (1985).
20. Feng, W. & Nansheng, D. Photochemistry of hydrolytic iron (III) species and photoinduced degradation of organic compounds. A minireview. *Chemosphere* **41**, 1137–1147 (2000).
21. McKay, C. P., Friedmann, E. I., Gómez-Silva, B., Cáceres, L., Andersen, D. T. & Landheim, R. Temperature and moisture conditions for life in the extreme arid region of the Atacama Desert: four years of observations including the El Niño of 1997–98. *Astrobiology* **3**, 393–406 (2003).
22. Anderson, K., Wells, S. & Graham, R. Pedogenesis of vesicular horizons, Cima Volcanic Field, Mojave Desert, California. *Soil Sci. Soc. Am. J.* **66**, 878–887 (2002).
23. Georgiou, C. D., Papapostolou, I. & Grintzalis, K. Superoxide radical detection in cells, tissues, organisms (animals, plants, insects, microorganisms) and soils. *Nat. Protoc.* **3**, 1679–1692 (2008).
24. Georgiou, C. D., Papapostolou, I., Sun, H. & McKay, C. P. Superoxide radical assays and applications in Mars-like Atacama soils. *J. Geophys. Res.* **112**, G04S13 (2007).
25. McCord, M. J. & Fridovich, I. Superoxide dismutase: an enzymic function for erythrocyte peroxidase (hemocuprein). *J. Biol. Chem.* **244**, 6049–6055 (1969).
26. Hyland, K. & Auclair, C. The formation of superoxide radical anions by a reaction between O₂, OH[•] and dimethyl sulfoxide. *Biochem. Biophys. Res. Com.* **102**, 531–537 (1981).
27. Sharma, K. S. *Inorganic Reaction Mechanisms* (Discovery Publishing House, 2007).
28. Makarov, S. Z. & Ladelnova, L. V. The peroxides of titanium, zirconium, and cerium formed in the reaction of their hydroxides with hydrogen peroxide. *Russian Chem. Bull.* **10**, 889–893 (1961).
29. Grintzalis, K., Zisimopoulos, D., Grune, T., Weber, D. & Georgiou, C. D. Method for the simultaneous determination of free/protein malondialdehyde and lipid/protein hydroperoxides. *Free Rad. Biol. Med.* **59**, 27–35 (2013).
30. Perez-Benito, J. F. Iron(III)-hydrogen peroxide reaction: kinetic evidence of a hydroxyl-mediated chain mechanism. *J. Phys. Chem.* **108**, 4853–4858 (2004).
31. Strlič, M., Kolar, J., Šelih, V.-S., Kočar, D. & Pihlar, B. A comparative study of several transition metals in Fenton-like reaction systems at circum-neutral pH. *Acta Chim. Slov.* **50**, 619–632 (2003).
32. Iuga, K., Olea, R. E. & Vivier-Bunge, A. Mechanism and kinetics of the OH[•] radical reaction with formaldehyde bound to an Si(OH)₄ monomer. *J. Mex. Chem. Soc.* **51**, 36–46 (2008).
33. Buxton, G. V., Greenstock, C. L., Helman, W. P. & Ross, A. B. Critical review of rate constants for reactions of hydrated electrons, hydrogen atoms and hydroxyl radicals (OH/O) in aqueous solution. *J. Phys. Chem. Ref. Data* **17**, 513–886 (1988).
34. Lybrand, R. A., Michalski, G., Graham, R. C. & Parker, D. R. The geochemical associations of nitrate and naturally formed perchlorate in the Mojave Desert, California, USA. *Geochim. Cosmochim. Acta* **104**, 136–147 (2013).
35. Michalski, G., Böhlke, J. K. & Thiemens, M. Long term atmospheric deposition as the source of nitrate and other salts in the Atacama Desert, Chile: new evidence from mass-independent oxygen isotopic compositions. *Geochim. Cosmochim. Acta* **68**, 4023–4038 (2004).
36. Zigah, D., Rodríguez-López, J. & Bard, A. J. Quantification of photoelectrogenerated hydroxyl radical on TiO₂ by surface interrogation scanning electrochemical microscopy. *Phys. Chem. Chem. Phys.* **14**, 12764–12772 (2012).
37. Xiao, Q. & Ouyang, L. Photocatalytic activity and hydroxyl radical formation of carbon-doped TiO₂ nanocrystalline: effect of calcination temperature. *Chem. Eng. J.* **148**, 248–253 (2009).
38. Ishibashi, K., Fujishima, A., Watanabe, T. & Hashimoto, K. Detection of active oxidative species in TiO₂ photocatalysis using the fluorescence technique. *Electrochem. Commun.* **2**, 207–210 (2000).
39. Li, Y.-F. & Liu, Z.-P. Particle size, shape and activity for photocatalysis on titania anatase nanoparticles in aqueous surroundings. *J. Am. Chem. Soc.* **133**, 15743–15752 (2011).
40. Anpo, M. et al. Generation of superoxide ions at oxide surfaces. *Top. Catal.* **8**, 189–198 (1999).
41. Daneshvar, N., Salari, D. & Khataee, A. R. Photocatalytic degradation of azo dye acid red 14 in water on ZnO as an alternative catalyst to TiO₂. *J. Photochem. Photobiol. A: Chem.* **162**, 317–322 (2004).
42. Zent, A. P., Ichimura, A. S., Quinn, R. C. & Harding, H. K. The formation and stability of the superoxide radical (O₂^{•-}) on rock-forming minerals: band gaps, hydroxylation state, and implications for Mars oxidant chemistry. *J. Geophys. Res.* **113**, E09001 (2008).
43. Buettnner, G. R. The pecking order of free radicals and antioxidants: lipid peroxidation, α-tocopherol, and ascorbate. *Arch. Biochem. Biophys.* **300**, 535–543 (1993).
44. Wilson, M. J. Sheet Silicates: Clay minerals. In: *Rock-forming minerals* (eds Deer, W. A., Howie, R. A. & Zussman, J.) Vol. 3C (The Geological Society, 2013).
45. Stoppato, C. & Bini, A. *Deserts (A Firefly Guide)* 1st edn (Firefly Books, 2003).
46. Watanabe, N., Kaneko, T., Uchimaru, Y., Yasumori, A. & Sugahara, Y. Preparation of water-dispersible TiO₂ nanoparticles from titanium tetrachloride using urea hydrogen peroxide as an oxygen donor. *Cryst. Eng. Comm.* **15**, 10533–10540 (2013).
47. Payne, H. J. & Foster, L. The action of hydrogen peroxide on carbohydrates. *J. Am. Chem. Soc.* **67**, 1654–1656 (1945).
48. Hall, S. J., Silver, W. L. & Amundson, R. Greenhouse gas fluxes from Atacama Desert soils: a test of biogeochemical potential at the Earth's arid extreme. *Biogeochemistry* **111**, 303–315 (2012).
49. Milne, P. J. & Zika, R. G. Amino acid nitrogen in atmospheric aerosols: Occurrence, sources and photochemical modification. *J. Atmos. Chem.* **16**, 361–398 (1993).
50. Patrick, R. & Golden, D. M. Kinetics of the reactions of amidogen radicals with ozone and molecular oxygen. *J. Phys. Chem.* **88**, 491–495 (1984).
51. Crowley, J. N. & Sodeau, J. R. Reaction between the amidogen radical, NH₂, and molecular oxygen in low-temperature matrixes. *J. Phys. Chem.* **93**, 4785–4790 (1989).
52. Sherman, D. M. in *Spectroscopic Characterization of Minerals and Their Surfaces* (eds Coyne, L. M., Blake, D. F. & McKeever, S. W. S.) ACS Symposium Series 415 (American Chemical Society, 1989).
53. Venkatchalapathy, R., Davila, G. P. & Prakash, J. Catalytic decomposition of hydrogen peroxide in alkaline solutions. *Electrochem. Commun.* **1**, 614–617 (1999).
54. Kelly, K. J., Sandoval, R. M., Dunn, K. W., Molitoris, B. A. & Dagher, P. C. A novel method to determine specificity and sensitivity of the TUNEL reaction in the quantitation of apoptosis. *Am. J. Physiol. Cell Physiol.* **284**, C1309–C1318 (2003).
55. Daniel Sheng, G., Xu, C., Xu, L., Qiu, Y. & Zhou, H. Abiotic oxidation of 17β-estradiol by soil manganese oxides. *Environ. Pollut.* **157**, 2710–2715 (2009).
56. Li, H., Lee, L. S., Schulze, D. G. & Guest, C. A. Role of soil manganese in the oxidation of aromatic amines. *Environ. Sci. Technol.* **37**, 2686–2693 (2003).
57. Quinn, R. C., Martucci, F. F., Miller, S. R., Bryson, C. E., Grunthaner, F. J. & Grunthaner, P. J. Perchlorate radiolysis on Mars and the origin of martian soil reactivity. *Astrobiology* **13**, 515–520 (2013).
58. Kounaves, S. P., Carrier, B. L., O'Neil, G. D., Stroble, S. T. & Clair, M. W. Evidence of martian perchlorate, chlorate, and nitrate in Mars meteorite EETA79001: Implications for oxidants and organics. *Icarus* **229**, 206–213 (2014).
59. Smith, M. L., Claire, M. W., Catling, D. C. & Zahnle, K. J. The formation of sulfate, nitrate and perchlorate salts in the martian atmosphere. *Icarus* **231**, 51–64 (2014).
60. Negron-Encarnacion, I. & Arce, R. Light-induced transformations of aza-aromatic pollutants adsorbed on models of atmospheric particulate matter: Acridine and 9(10-H) acridone. *Atmos. Environ.* **41**, 6771–6783 (2007).
61. Khan, A. U. & Kasha, M. Singlet molecular oxygen in the Haber-Weiss reaction. *Proc. Natl Acad. Sci. USA* **91**, 12365–12367 (1994).
62. Mao, Y., Zang, L. & Shi, X. Singlet oxygen generation in the superoxide reaction. *Biochem. Mol. Biol. Int.* **36**, 227–232 (1995).
63. Mattimore, V. & Battista, J. R. Radioresistance of *Deinococcus radiodurans*: functions necessary to survive ionizing radiation are also necessary to survive prolonged desiccation. *J. Bacteriol.* **178**, 633–637 (1996).
64. Daly, M. J. et al. Protein oxidation implicated as the primary determinant of bacterial radioresistance. *PLoS Biol.* **5**, e92 (2007).
65. Oyama, V. I., Berdahl, B. J. & Carle, G. C. Preliminary findings of the Viking Gas Exchange Experiment and a model for Martian surface chemistry. *Nature* **265**, 110–114 (1977).
66. Klein, H. P. The Viking biological experiments on Mars. *Icarus* **34**, 666–674 (1978).
67. Zent, A. P. & McKay, C. P. The chemical reactivity of the martian soil and implications for future missions. *Icarus* **108**, 146–457 (1994).
68. Hecht, M. H. et al. Detection of perchlorate and the soluble chemistry of Martian soil at the Phoenix Lander Site. *Science* **325**, 64–67 (2009).
69. Glavin, D. P. et al. Evidence for perchlorates and the origin of chlorinated hydrocarbons detected by SAM at the Rocknest aeolian deposit in Gale Crater. *J. Geophys. Res.* **118**, 1–19 (2013).
70. Linxiang, L. et al. An HPLC assay of hydroxyl radicals by the hydroxylation reaction of terephthalic acid. *Biomed. Chromatogr.* **18**, 470–474 (2004).

Acknowledgements

C.D.G. was financially supported by the Greek Ministry of Education. H.J.S. and G.Z. were supported by a grant from the NASA Astrobiology Program NNX07AT65. H.J.S. was also in part supported by the National Science Foundation under grant number IIA-1301726. He thanks R. Kreidberg for editorial assistance. C.P.M. acknowledges the support from the NASA Planetary Protection Program. We thank the ESRF for the provision of synchrotron X-ray beamtime at the high-resolution powder diffraction beamline (ID31). We are grateful to Professor P.V. Ioannou (Department of Chemistry) and Associate Professor M. Kornaros (Department of Chemical Engineering) at the University of Patras, Greece, for HTPA synthesis and HPLC-MS identification in samples, respectively.

Author contributions

C.D.G., H.J.S. and C.P.M. conceived and designed the experiments, analysed the data, contributed materials/analysis tools and co-wrote the paper. C.D.G. conceived the soil O_2^- /peroxide and $\cdot OH$ detection assays and experimentally developed and performed

them with K.G., I.P., D.Z and K.P. H.J.S. and G.Z. also performed soil peroxide detection experiments. K.G., I.P., D.Z and K.P. had equal contribution in this study. E.K., G.E.C. and I.M. designed and performed the mineralogical experiments, and analysed the relevant data.

Additional information

Supplementary Information accompanies this paper at <http://www.nature.com/naturecommunications>

Competing financial interests: The authors declare no competing financial interests.

Reprints and permission information is available at <http://npg.nature.com/reprintsandpermissions/>

How to cite this article: Georgiou, C. D. *et al.* Evidence for photochemical production of reactive oxygen species in desert soils. *Nat. Commun.* 6:7100 doi: 10.1038/ncomms8100 (2015).